RSC Advances

REVIEW

View Article Online
View Journal | View Issue

Cite this: *RSC Adv.*, 2016, **6**, 31988

Morphology controllable syntheses of micro- and nano-iron pyrite mono- and poly-crystals: a review

Haiyang Xian,[abc] Jianxi Zhu,*[ab] Xiaoliang Liang[ab] and Hongping He[ab]

Received 24th February 2016
Accepted 19th March 2016

DOI: 10.1039/c6ra04874a

www.rsc.org/advances

Synthesis of iron pyrite with defined morphology has long been actively pursued, due to the strong size and shape dependence of their chemical and physical properties. This review provides comprehensive information outlining current knowledge regarding the morphology controllable syntheses of micro- and nano-iron pyrite mono- and poly-crystals. The wet-chemical methods are summarized as the controllable syntheses, including the hydrothermal, solvothermal, hot-injection and heating-up methods, sulphidation and methods with other relatively high efficiencies. The present study reveals the discussion of relationship between the morphologies and major controlling factors, the temperature, precursor chemicals, solvents and surfactants. The existing challenges for future fine tuning of iron pyrite facets are also proposed for improving the performance of iron pyrite based materials.

1. Introduction

Iron pyrite is a common type of sulphide mineral and is also known as "fool's gold"; however, its various applications make it a promising material in the energy storage and environmental protection areas. It is a very attractive candidate for the next generation photovoltaic material, due to its high absorption coefficient and its energy band gap ($E_g \approx 0.95$ eV), which is appropriate for photovoltaic energy conversion.[1–8] Not only could pyrite affect the environment in which it is present through its surface reactivity,[9] but it has also been widely used in environmental applications for heavy metal adsorption, reduction or related processes.[10–20]

The atomic structure of iron pyrite (Fig. 1) is well-known and was first determined by Bragg[21] with his new X-ray diffraction system in 1914. The structure of iron pyrite is an analogy of the NaCl-type structure. The disulphide dumbbells S_2^{2-} groups are situated at the Cl^- positions, *i.e.* at the cube centre and the midpoints of cube edges, and the ferrous ion atoms at the Na^+ positions, *i.e.* the corners and face centres. Regarding the arrangement of the disulphide dumbbells, the symmetry of pyrite structure, *Pa*3, is lower than that of NaCl-type structure, *Fm*3*m*. The space group of pyrite determines its crystal habit, leading to the most common shapes of its crystals are {100}, {111} and {210} facets in nature.[22]

Chemical reactions always occur on the surfaces, and different shapes of crystals present different surfaces, therefore, the synthesis of transition metal dichalcogenides MX_2 (M = Fe, Co, Ni, Cu, Zn; X = S, Se) with the pyrite structure and defined morphology has long been actively pursued.[23] For iron pyrite, the morphology is significant to its surface reactivity or potential applications, *e.g.* solar cells and lithium batteries, and environmental protection. This is attributed to the fact that all these applications are mainly based on the surface characteristics of iron pyrite, which are determined by its morphology.

The consideration of morphology controllable syntheses of iron pyrite has been brought into attention for nearly two decades. Many synthetic routes to iron pyrite have been suggested since the first synthesis of iron pyrite, which were designed to investigate the formation of iron pyrite through the hydrothermal method in 1912.[24] So far, hydrothermal, solvothermal, hot-injection, heating-up, low temperature aqueous, sulphidation

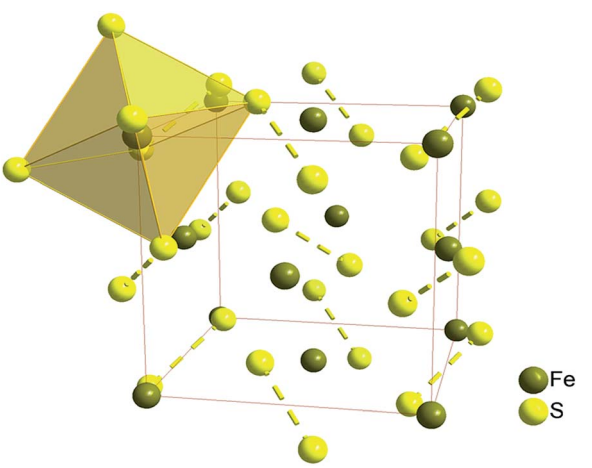

Fig. 1 Representation of the iron pyrite atomic structure.

[a]*Key Laboratory of Mineralogy and Metallogeny, Guangzhou Institute of Geochemistry, Chinese Academy of Sciences, Guangzhou 510640, Guangdong, People's Republic of China. E-mail: zhujx@gig.ac.cn*

[b]*Guangdong Provincial Key Laboratory of Mineral Physics and Materials, Guangzhou 510640, Guangdong, People's Republic of China*

[c]*University of Chinese Academy of Sciences, Beijing 100049, People's Republic of China*

and vapour growth syntheses are the main synthetic routes to iron pyrite. Among these methods, the hydrothermal, solvothermal, hot-injection, heating-up and low temperature aqueous routes could be classified into one group, namely the wet-chemical routes. Compared to others, the wet-chemical and sulphidation routes are much more suitable to materialize the morphological controlling of synthetic iron pyrite.

To the best of our knowledge, however, the experimental syntheses of iron pyrite framboids have only been examined in one review study,[25] the purpose of which was to determine the formation mechanism of iron pyrite framboid texture. There has been no comprehensive review which would particularly discuss about the controllable syntheses of iron pyrite. In this review study, it was attempted to link the reported literature sources and draw the outline of current knowledge about morphology controllable syntheses of micro-nano iron pyrite mono- and poly-crystals. This review will not focus on the syntheses of polycrystalline thin films, their properties or applications, as these features are being rapidly developing and would constitute a much larger review paper. This review focuses on the progress made in the field of morphology controllable syntheses of iron pyrite mono- and poly-crystals.

2. Wet-chemical syntheses of shape-controlled iron pyrite

2.1 Hydrothermal synthesis

The hydrothermal method can be defined as a method for the synthesis of crystals that depends on solubility of minerals in hot water, at a temperature always higher than 100 °C, under high pressure.[26] The synthesis is always performed in an apparatus consisting of a steel vessel, which is always termed as an autoclave. In the autoclave, some certain nutrient, which always contains all the elements for a certain kind of desired crystal, is supplied along with water. A temperature gradient is maintained between the dissolution and growth zones of the designed crystals. At the end with the higher temperature the nutrient solute dissolves, while at the cooler end it nucleates and grows to crystals.

During the past decade, many hydrothermal routes, based on the polysulphide synthesis pathway, have been carried out to synthesize iron pyrite crystals. Many types of chemicals, such as $FeSO_4$,[27–30] $FeCl_3$,[8,31,32] $FeCl_2$,[33,34] Na_2S,[31,32] $Na_2S_2O_3$ [28,30] and S,[28,29] were used as precursors. In general, the Fe and S based sources came from different precursors, but some chemicals, such as iron diethyldithiocarbamate ($Fe(S_2CNEt_2)_3$),[35] contain both S and Fe were considered as the single source of Fe and S for synthesizing iron pyrite. All the published hydrothermal experiments of the past decade are summarized in Table 1. It can be observed that the Fe source usually comes from one chemical, while the S source from more than one, in the majority of the previous studies.

Different starting materials may lead to different shapes of the synthetic iron pyrite crystals. From the published reports, it can be observed that iron pyrite single crystals with certain facets could not always be obtained, when $Na_2S_2O_3$ and elemental sulphur were selected as the S precursors. However, certain conditions, faceted iron pyrite crystals were able to be

Table 1 Iron pyrite from reported hydrothermal synthesis

Reactant	Surfactant	T & t	Shape	Ref
$FeSO_4 \cdot 7H_2O$ + thiourea	PVP[a]	200 °C for 40 h	Particle	27
$FeSO_4 \cdot 7H_2O + Na_2S_2O_3$ + S		200 °C for 24 h	Framboid	28
$Fe(S_2CNEt_2)_3$		180 °C for 12 h	Cube	35
$FeSO_4 + Na_2S_2O_3$ + S		200 °C for 24 h	Polyhedron	29
Fe foil + S		160 °C for 12 h	Nanosheet	36
$[(C_2H_5O)_2P(S)S]_3Fe$	CTAB[b]	200 °C for 12 h	Quasi-cube	37
$FeCl_3 \cdot 6H_2O + Na_2S \cdot 9H_2O$ + 5S	PEG-400[c]	180 °C for 20 h	Polyhedron	31
$FeCl_2 \cdot 4H_2O$ + S	PVP[a] + PVA[d]	453 K for 12 h	Cube	33
$FeCl_2 \cdot 4H_2O$ + S	PVP[a] + PVA[d]	453 K for 12 h	Octahedron	33
$FeSO_4 \cdot 7H_2O + Na_2S_2O_3$ + S		200 °C for 24 h	Particle	30
$FeSO_4 \cdot 7H_2O + Na_2S_2O_3$ + S	CTAB[b]	200 °C for 24 h	Sphere-like	30
$FeCl_2 \cdot 4H_2O$ + 2S	PVP[a]	200 °C for 24 h	Cube	34
$FeCl_3 \cdot 6H_2O$ + SDS + $Na_2S \cdot 9H_2O$		180 °C for 18 h	Flower like	8
$FeCl_3 \cdot 6H_2O$ + S + Na_2S + iron foil		160 °C for 6 h	Cube	32
$Fe(acac)_3 + Na_2S_2O_3 \cdot 5H_2O$ + S	OTA[e] + EA[f]	220 °C for 12 h	Ellipsoid-like	38
Nano-$Fe_3O_4 + Na_2S_2O_3 \cdot 5H_2O$ + S	OTA[e] + EA[f]	220 °C for 12 h	Ellipsoid-like	38
$FeSO_4 \cdot 7H_2O + Na_2S \cdot 9H_2O$ + S		160 °C for 3–24 h	Cube	39 and 40
$FeSO_4 + Na_2S_2O_3$		180 °C for 4 h	Spherical shape	41
$FeCl_3$ + Na_2S + S	PEG-400[c]	120 °C for 48 h	Coagulation	42
Fe + S	CTAB[b]	200 °C for 24 h	Spheroid shape	43
$Fe(NO_3)_3$ + L-cysteine	ETA[g] : H_2O = 8 : 1	200 °C for 48 h	Cube	44
$Fe(NO_3)_3$ + L-cysteine	ETA[g] : H_2O = 1 : 1	200 °C for 48 h	Flake-like	44
$Fe(NO_3)_3$ + L-cysteine	ETA[g] : H_2O = 1 : 8	200 °C for 48 h	Tetrakaidecahedron	44
$FeCl_2 \cdot 4H_2O$ + S	Gelatin	200 °C for 48 h	Particle	45

[a] As polyvinylpyrrolidone. [b] As hexadecyltrimethylammonium bromide. [c] As polyethylene glycol. [d] As polyvinyl alcohol. [e] As 1-octylamine. [f] As ethanol. [g] As ethanolamine.

synthesized when the precursors were without $Na_2S_2O_3$. Thus, it can be concluded that both the precursor and the hydrothermal conditions can control the shape of iron pyrite.

From Table 1, it can also be observed that two sulphur-containing chemicals have always been preferred as the S sources to synthesize iron pyrite. One is elemental sulphur and the other is $Na_2S_2O_3$ or Na_2S. Wu *et al.*,[28] Feng *et al.*,[29] Zhang *et al.*[30] and Xia *et al.*[38] used $Na_2S_2O_3$ and elemental sulphur as the S precursors to synthesize iron pyrite at hydrothermal conditions. The iron pyrite samples they obtained contained irregular particles or aggregation of polyhedrons. Zou *et al.*,[31] Middya *et al.*[42] and Yang *et al.*[39,40] used Na_2S and elemental sulphur as the S precursors. Particularly at Yang *et al.*'s work,[39,40] they initially prepared Fe solution with $FeSO_4 \cdot 7H_2O$ + $Na_2S \cdot 9H_2O$ and S solution with $Na_2S \cdot 9H_2O$ + S; the S solution was heated to 100 °C until no residual sulphur was remaining, and then mixed the prepared solutions into an autoclave to perform the hydrothermal experiments. The iron pyrite they obtained was of cubic shape, however, the surface of the cube was relatively rough. Kush *et al.*[8] used $FeCl_3 \cdot 6H_2O$, sodium dodecyl sulfonate and $Na_2S \cdot 9H_2O$ as precursor and flower-like iron pyrite particles were obtained. Qiu *et al.*[32] prepared a precursor solution, mixed with $FeCl_3 \cdot 6H_2O$, S powder and Na_2S, and the resulting suspension reacted with a piece of clean iron foil in a hydrothermal system. The products they obtained were uniformly distributed cubes with smooth surfaces (Fig. 2a).

When comparing the number of S sources to synthesize iron pyrite, the one S source may be much easier to operate in the hydrothermal experiments, *versus* two S sources. Hu *et al.*[36] and Wang *et al.*[33] only used one S chemical, *i.e.* elemental sulphur, during the hydrothermal process and their results appear more interesting than those employed two S sources. For instance, Hu *et al.*[36] synthesized FeS_2 nanosheet films on iron substrates through a one-step hydrothermal treatment of iron foil and sulphur powder. Fig. 2b reveals that the thin iron pyrite nanosheets transformed into flower-like and the thicknesses of the nanosheets were approximately 30 nm. Wang *et al.*[33] obtained cube-shaped and octahedron-shaped iron pyrite crystals (Fig. 3) by employing polyvinylpyrrolidone (PVP) and polyvinyl alcohol (PVA) as surfactant and by simply adjusting the NaOH concentration. And the size of the product can be adjusted by varying the reaction parameters.

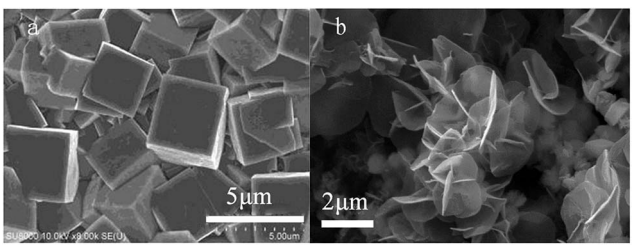

Fig. 2 FESEM images of (a) cubic iron pyrite film obtained in ref. 32 and (b) thin iron pyrite nanosheets transformed into flower-like in ref. 36. (a) is reprinted from ref. 32. Copyright 2013 Royal Society of Chemistry; (b) is reprinted with permission from ref. 36. Copyright 2008 American Chemical Society.

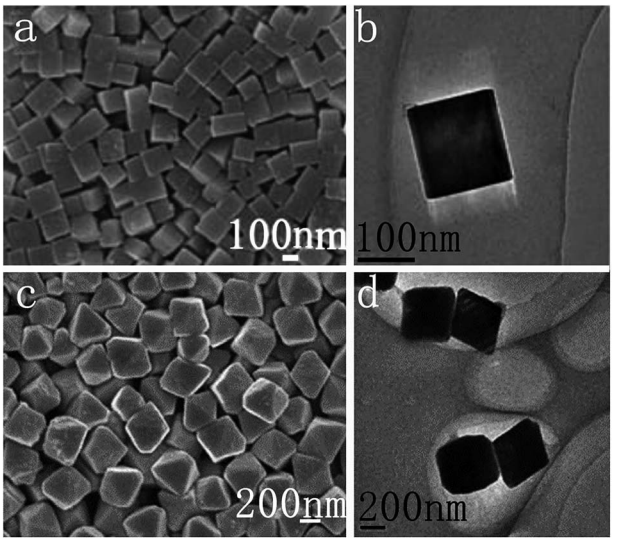

Fig. 3 SEM (a and c) and TEM (b and d) images of the cube-shaped and octahedron-shaped iron pyrite crystallites.[33] Reprinted with permission from ref. 33. Copyright 2010 Royal Society of Chemistry.

Cubic iron pyrite crystals could be synthesized *via* a single-source approach. Chen *et al.*[35] synthesized cubic FeS_2 crystals by using iron diethyldithiocarbamate as precursor. Wadia *et al.*[37] approached their synthesis procedure by beginning with the formation of the single source molecular precursor iron(III) diethyl dithiophosphate ($[(C_2H_5O)_2P(S)S]_3Fe$) in aqueous solution through the reaction between iron(III) chloride ($FeCl_3$) and diethyl dithiophosphate ammonium salt ($(C_2H_5O)_2P(S)SNH_4$). Following, the single source precursor, with the addition of hexadecyltrimethylammonium bromide (CTAB) acting as a surfactant, undergoes thermal decomposition by a hydrothermal reaction. The prepared pyrite had the morphology of quasi-cubic nanocrystal agglomerations.

Surfactants always play an important role in shape controlling during crystal growth. It is well established that the shape evolution of crystals during growth in a given environment is largely driven by the inherent necessity of minimizing the total surface energy.[46] The computed relaxed surface energies of pyrite (100), (111), (210) and (110) surfaces are 1.06, 1.40, 1.50 and 1.68 J m^{-2}, respectively.[47,48] Since the surface energy of the (100) is the lowest, the most common naturally and synthetically occurring pyrite surface is (100). The surface energy may decrease with the selective adsorption of appropriate molecules and/or ions on certain surfaces. It consequently leads to the growth rate of different surfaces can be controlled by using different adsorbates.

Although various types of surfactants have been supplied in synthesis of pyrite,[27,30,31,33,34,37,38,42,43,45] only a few obtained the {100} and/or {111} facets.[33,34] No facets have been synthesized by employing CTAB and all the pyrite crystals synthesized with CTAB tend to form aggregations.[30,37,43] However, regarding PVP, it can be used as a surface capping agent to bind the iron atoms at the (111) surface and direct the formation of {100} facets. Compared to the amount of previous studies in order to synthesize other synthetic crystals with specific facets,[49] it is

relatively feebler to work for the synthesis of iron pyrite. Hence, some appropriate capping agents should be carried out to synthesize iron pyrite with specific facets and this should be emphasized in the future research on iron pyrite synthesis.

The pH may be another important factor in controlling the iron pyrite shape during the hydrothermal processes. However, limited studies have been focused on pH.[33,38,39,42] From these studies, it can be easily found that iron pyrite crystals could easier form regular shapes in an acidic environment[38] than in alkaline.[33,39] Combined with the surfactant of PVP and PVA, the iron pyrite shape can be controlled by only adjusting the NaOH concentration, *i.e.* the pH.[33] However, the mechanism that describes the effect of pH on the synthesis of iron pyrite is still unknown.

2.2 Solvothermal synthesis

Solvothermal synthesis is similar to hydrothermal synthesis, where the synthesis is also conducted in a stainless steel autoclave. The only difference between both routes could be that the precursor solution of the solvothermal method is usually an organic solvent instead of aqueous, as in hydrothermal method. Table 2 summarizes the synthesis of iron pyrite from reported solvothermal syntheses. It can be observed that ethylenediamine, benzene, ethanediol and ethanol are usually used as the precursor organic solvent. To produce iron pyrite by the solvothermal synthesis method, E'jazi and Aghaziarati[50] used various solvents including ethanol, 1-propanol, 2-propanol, 1-butanol and ethylenediamine. Their results showed that ethanol and 1-butanol were fairly appropriate to prepare iron pyrite.

Various types of solvents are chosen as the reaction media, which is due to the fact that the precursor organic solvent could be the shape controller during the solvothermal synthesis of iron pyrite. Qian *et al.*[51] synthesized nano rod-like and spherical iron pyrite crystals by using ethylenediamine (EDA) and benzene, respectively, as the precursor solvent during solvothermal processes. When EDA is employed as the reaction media, regardless the precursor chemicals or the reaction parameters used, iron pyrite tends to grow into one-dimensional shape, nano wires and nano rods, which is affirmed by Kar *et al.* (Fig. 4).[52,53] To perform selective synthesis of air-stable, phase-pure iron pyrite nano cubes, spheroidal nanocrystals and microspheres, Yu *et al.*[54] utilized 1-octylamine and 1-octanol as the precursor solvent. Nano cubes and nano- and micro-spheres were obtained. Furthermore, when ethanediol[55] and ethylene glycol[56] were used, the shape of iron pyrite had the morphology of polyhedrons and spheres, but the surface index of the polyhedron was hard to identify.

However, the mechanism of the organic solvent effect on the morphology of iron pyrite is still unknown, although many

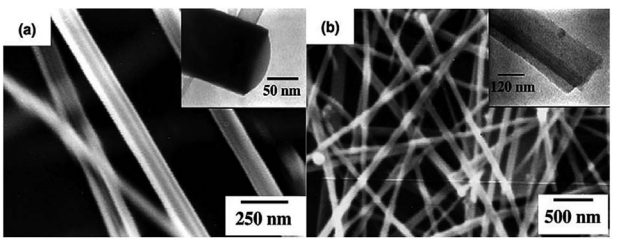

Fig. 4 Nanocrystalline FeS_2 with different morphologies, synthesized by using $Fe(NO_3)_3 \cdot 9H_2O$ at 180 °C with different molar concentration of the precursors: (a) less amount (half) of the precursor; (b) higher molar concentration (double) of the precursors.[52] Reprinted with permission from ref. 52. Copyright 2004 Elsevier.

Table 2 Iron pyrite from reported solvothermal syntheses

Reactant	Solvent & surfactant	T & t	Shape	Ref
$FeSO_4 \cdot 7H_2O + Na_2S_3$	Ethylenediamine Benzene	130 °C, 8–12 h	Nanorod Nanoparticle	51
$FeSO_4 \cdot 7H_2O$ + thiourea	Ethylenediamine	180–230 °C, 12 h	Nano rod	52
$FeCl_3$ + thiourea	Ethylenediamine		Micro rod	
$Fe(NO_3)_3 \cdot 9H_2O$ + thiourea	Ethylenediamine		Nanowire	
$FeSO_4$ + thiourea	Alcohol–water + PVP[b]	200 °C, 36 h	Nanoparticle	57
$Fe(NO_3) \cdot 9H_2O + Na_2S$	Ethylenediamine	180 °C, 12 h	Nanowire	53
$FeCl_2 \cdot 4H_2O$ + S	Ethylene glycol + TX-100[c] Ethylene glycol + PVP[b]	180 °C, 12 h	Cube Octahedron	58
$FeSO_4 \cdot 7H_2O$ + thiourea	Ethanol–water + PVP[b]	180 °C, 36 h	Polyhedron	59
$Fe(NO_3)_3 \cdot 9H_2O$ + thiourea	Ethanediol	200 °C, 24 h	Sphere	55
$FeCl_3 \cdot 6H_2O$ + S	Ethylene glycol + DMF[d]	160 °C, 12 h	Sphere	56
Various[a]	Various[e]	160–200 °C, 5 h	Irregular	50
Potassium ferrocyanide + S	Alcohol + PVP[b]	200 °C, 20 h	Particle	60
$FeCl_2$ + S	OLA[f] + 1,2-dodecanediol	180 °C, 18 h	Cube	61
FeE_3 + S	Various[g]	190 °C, 3–22 h	Nano particle	62
Fe_2O_3 + S	1-Octylamine + 1-octanol 1-Octylamine 1-Octanol	260 °C	Spheroidal Nanocube Microsphere	54

[a] As $FeSO_4 \cdot 7H_2O$, $Fe(NO_3)_3 \cdot 9H_2O$, $FeCl_3 \cdot 6H_2O$, thiourea, Na_2S and Na_2SO_3. [b] As polyvinylpyrrolidone. [c] As Triton X-100. [d] As dimethyl formamide. [e] As ethanol, 1-propanol, 2-propanol, 1-butanol and ethylenediamine. [f] As oleylamine. [g] As octadecylamine, toluene, dimethylformamide, octadecylxanthate, dodecylamine, oleylamine and trioctylphosphine oxide.

experiments show that the organic solvent could control the shape. It is only empirically evident that some kinds of solvent are suitable for certain morphologies. Therefore, before performing the substantial morphology controlling of iron pyrite through the organic solvent route, additional research studies should be carried out to ascertain the mechanism.

Not only could the precursor solvent affect the shape of products from the solvothermal routes, but also other parameters, such as surfactant, pH, Fe precursor, could control the growth of iron pyrite crystals. Similar to the hydrothermal processes, surfactant is also an important factor in the iron pyrite growth processes. Octadecylamine (ODA), octadecylxanthate (ODX), dodecylamine (DDA), oleylamine (OLA) and trioctylphosphine oxide (TOPO) were employed as surfactants,[62] which have been confirmed to be suitable for obtaining iron pyrite colloid. PVP,[57–60,63] Triton X-100,[58] dimethyl formamide (DMF)[56] and 1,2-dodecanediol[61] were also proposed to control the shape of iron pyrite. Liu *et al.*[60] and Liu *et al.*[61] obtained iron pyrite cubic and irregular particles by using 1,2-dodecanediol and PVP as surfactant, respectively. Wang *et al.*[56,58] successfully synthesized cubic, octahedron and spherical iron pyrite by using Triton X-100, PVP and DMF as surfactant, respectively. However, regular iron pyrite crystals were not only obtained due to the surfactant, but also NaOH concentration played a significant role.[58]

2.3 Hot-injection synthesis

The first hot-injection synthesis for cadmium chalcogenide nanocrystals was reported by Murray *et al.*[64] in 1993. Later, this hot-injection method was extended to the synthesis of nanocrystals for various materials,[65] including some metal sulphides (PbS, ZnS, CdS and MnS).[66] However, regarding iron pyrite synthesis, the first attempt to use this method was reported 18 years later, in 2011.[2,5,67]

The hot-injection process involves two stages, the nucleation and the kinetically controlled growth. The quick injection of the precursor leads to a large supersaturation degree in the growth solution, which results in the formation of nuclei, releasing the excess of free energy present in the system. The nuclei formation in the growth solution reduces the supersaturation degree and thus the precursor concentration below a critical value, at which the nucleation stage is completed and the crystal growth stage begins. The rapidly injection process leads to the formation and crystals growth of all the nuclei almost at the same conditions, therefore, the hot-injection synthesis could lead to the monodisperse crystals.[68]

In a typical synthesis of iron pyrite by hot-injection method, the experiments are always carried out under inert atmosphere (usually Ar or N_2), which is performed by standard Schlenk line techniques.[2,5] The whole process mainly includes four steps.[67–69] First, the sulphur and iron precursor solution is prepared in separate vessel, at certain temperature. Second, one of the prepared solutions of the precursor are rapidly injected into the other at the designated temperature (always higher than 100 °C). Third, after the injection, the reaction system is heated up to a constant temperature for different aging times, which always ranges from several minutes to hours. Finally, following cooling of the reaction system to ambient temperature, the precipitate is washed and collected *via* centrifugation. Table 3 summarizes the reported hot-injection syntheses of iron pyrite.

From Table 3, it can be observed that the injection processes could be divided into two classes, one involving injecting the sulphur solution into the iron solution, while the other requires injecting the iron solution into the sulphur solution. However, the majority of the reported processes are classified into the first class, while only one case[70] is classified to the second. It can also be observed that elemental sulphur and $FeCl_2$ were employed as the sulphur and iron precursors, in the majority of the reported experiments. Only some cases used iron pentacarbonyl[70] and $FeBr_2$ (ref. 71) as iron precursors. In most cases, OLA is often chosen as the reaction media due to its higher boiling point, commercial availability, and relatively low cost, compared to other alkylamines. Except for OLA, some other types of organic solvent, such as diphenyl ether (DE) or ODA, were also used in the iron pyrite hot-injection synthesis.

Combined with organic solvent, surfactants could affect the shape and size of iron pyrite. TOPO was firstly employed as surfactant to control the shape of iron pyrite in hot-injection syntheses. The prepared iron pyrite has cubic shape. The size of iron pyrite nanocrystals can be set between 60 and 200 nm by adjusting the amount of TOPO.[2] In addition to TOPO, 1,2-hexanediol[71] and 1-hexadecanesulfonate[72] could be employed as surfactants to control the shape of iron pyrite. According to Bhandari *et al.*'s work,[71] compared to TOPO, when 1,2-hexanediol is employed as capping ligands, the cubic iron pyrite could also be obtained. Lucas *et al.*[72] ascertained 1-hexadecanesulfonate as an efficient ligand to synthesize cubic iron pyrite nanocrystals, by attempting phenyl diamines and high molecular weight surfactants, such as PVP and Triton X-100. However, neither shape nor size controlling were achieved.

With the hot-injection method, different shapes of iron pyrite can be obtained, such as cubes, dendrites, sheets or plates, all in the nanoscale. Following injection, the initial iron pyrite monomer concentration is an important role in controlling the shape of iron pyrite. Li *et al.*[67] obtained iron pyrite nanocubes and nanodendrites by adjusting the precursor concentration, which results in different monomer concentration. Ge *et al.*[77] also concluded that increasing the monomer concentration changes the shape of the final particles from nanocubes to nanoplates and finally to spheres.

The thermodynamic conditions are also a significant factor for synthesizing iron pyrite by the hot-injection method. Kirkeminde *et al.*[76] reported the thermodynamically controlled synthesis of FeS_2 nanocrystals, depending on the reaction temperature and chemical precursors. Similarly, Gong *et al.*[73] also obtained iron pyrite cubes and nanosheets by changing the injection temperature. Fig. 5a–h displays a sequence of TEM images for the formation process of iron pyrite cubes and sheets. Kirkeminde *et al.*[76] proposed an energy model for the formation of two different crystal faces for iron pyrite, the {100} and {111}. This model explains the energy aspect of the formation of iron pyrite at the {100} and {111}. However, it could not provide further information on how the iron pyrite nanocubes or nanospheres form. Hence, Oriented Attachment (OA), which appears

Table 3 Iron pyrite syntheses from reported hot-injection synthesis

Reaction system[a]	Atm	T, t[b]	Shape	Ref
S(OLA[c]) → $FeCl_2$(OLA[c], 170 °C) + TOPO[j]	N_2	220 °C, 2 h	Nanocube	2
S(OLA[c]) → $FeCl_2$(OLA[c], 100 °C)	N_2	220 °C, 20 min	Nanodendrite; nanocube	67
S(DE[d]) → $FeCl_2$(ODA[e], 120 °C)	Ar	220 °C, 3 h	Nanoparticle	5
S(DE[d]) → $FeCl_2$(ODA[e], 100 °C)	N_2	200 °C, 1 h	Nanocube	69
$Fe(CO)_5$ → S(OLA[c], 120 °C)	Ar	120–240 °C, 4 h	Nanoplate	70
S(OLA[c]) → $FeCl_2$(OLA[c] + HDDO[l] + ODE[m], 100 °C)	N_2	240 °C, 1 h	Nanoparticle	74
S(DE[d]) → $FeCl_2$(ODA[e], 120 °C)	Ar	220 °C, 2 h	Nanocube	73
		145 °C, 2 h	Nanosheet	73
S(OLA[c]) → $FeCl_2$(OLA[c], 150 °C)	N_2	250 °C, 30 min	Nanoparticle	75
S(DE[d]) → $FeCl_2$(ODA[e], 120 °C)	Ar	220 °C, 90 min	Cube	76
S(DE[d]) → $FeCl_2$(ODA[e], 170 °C)	Ar	220 °C, 90 min	Popcorn-shaped	76
S(DE[d]) → $FeCl_2$(ODA[e], 220 °C)	Ar	220 °C, 90 min	Nanosphere	76
S(DE[d]) → $Fe(acac)_2$(ODA[e], 220 °C)	Ar	220 °C, 90 min	Hexagonal sheet	76
S(DE[d]) → $Fe(CO)_5$(ODA[e], 120 °C)	Ar	220 °C, 90 min	Hexagonal sheet	76
S(OLA[c] + HSAS[f]) → $FeCl_3$(OLA[c], 120 °C)	N_2	220 °C, 10 min	Cube	72
S(OLA[c]) → $FeCl_2$(OLA[c], 115 °C) + TOPO[j]	N_2	230 °C, 2 h	Nanoparticle	4
S(OLA[c]) → $FeCl_2$(OLA[c], 110 °C)	N_2	180 °C, 5 min to 6 h	Nanoparticle; nanoplate	77
S(DDA[g]) → $FeCl_2$(DDA[e], 95 °C)	Ar	215 °C, 1 h	Nanoparticle	78
S(DE[d]) → $FeCl_2$(ELA[h], 115 °C)	N_2	210 °C, 1 h	Particle husk	79
S(OLA[c]) → $FeCl_2$(OLA[c], 115 °C)	N_2	230 °C, 2 h	Cube	3
S(DE[d]) → $FeCl_2$(ODA[e] + PL[i], 220 °C)	N_2	205 °C,	Nanocube	80
S(OLA[c]) → $FeCl_2$(OLA[c], 100 °C)	N_2	220 °C, 3 h	Nanoparticle	81
S(DE[d]/OLA[c]) → $FeCl_2$(ODA[e]/OLA[c], 120 °C)	N_2	120 °C, 30 min	Nanorod	82
		220 °C, 2 h	Quasi-cube	82
S(OLA[c]) → $FeBr_2$(OLA[c], 120 °C) + TOPO[j]/HDO[k]	N_2	220 °C, 2 h	Cube	71
S(OLA[c]) → $FeCl_2$(OLA[c], 90 °C)	N_2	180–260 °C, 1–24 h	Cube	83
S(DE[d]) → $FeCl_2$(ODA[e], 120 °C)	Ar	200 °C for 3 h	Rod	84
S(DE[d]) → $FeCl_2$(ODA[e]/OLA[c], 120 °C)	N_2	220 °C, 2 h	Nanoparticle	85

[a] Sign on the left of the arrow stands for the injection solution; sign on the right hand of the arrow, in the parenthesis, stands for the injected solution and the injection temperature, and surfactant, out of the parenthesis. [b] T and t are aging temperature and time after injection. [c] As oleylamine. [d] As diphenyl ether. [e] As octadecylamine. [f] As 1-hexadecanesulfonic acid sodium salt. [g] As dodecylamine. [h] As ethanolamine. [i] As paraffin liquid. [j] As trioctylphosphine oxide. [k] As 1,2-hexanediol. [l] As 1,2-hexadecanediol. [m] As octadecene.

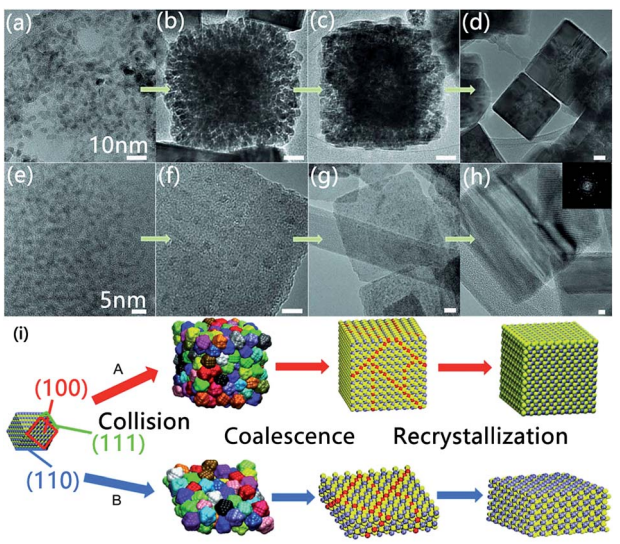

Fig. 5 Sequences of TEM images, showing the detail of the attachment process: (a) FeS_2 QD seeds; (b) seed collision; (c) seed coalescence; (d) recrystallization process from polycrystal to monocrystal. (e–h) FeS_2 seeds evolved into single crystal nanosheet by coalescence and recrystallization process and (i) schematic illustration of the cubic (pathway A) and sheet (pathway B) formation of FeS_2 nanocrystals.[73] Reprinted from ref. 73. Copyright 2013 Macmillan Publishers Limited.

to be a suitable mechanism during the development of nanoscale materials, was introduced in iron pyrite crystalline growth by Gong *et al.*[73] and Zhu *et al.*[85] They utilized the OA mechanism (Fig. 5i) to interpret the iron pyrite cubes and spheres[73] and the anisotropic growth of iron pyrite,[85] respectively.

However, the driving force of the OA mechanism for iron pyrite synthesis is still unknown. It would be interesting to know how the different facets combined with each other and does the driving force come from the surfactants. If so, the thing more interesting is how the surfactants work on the surface. Therefore, there is a long way to go into the mechanism of iron pyrite synthesis by hot-injection routes.

2.4 Heat-up synthesis

The heat-up synthesis is also an important method for the synthesis of iron pyrite nanocrystals. Compared to hot-injection synthesis, the heat-up method appears much more practical. The reaction system is heated up directly from room temperature to reaction temperature. In the reaction system, many types of organic solvents, which are also used in the hot-injection synthesis, are employed.

There are limited reports about the iron pyrite synthesis from the heat-up method, which are summarized in Table 4. It

Table 4 Iron pyrite from reported heat-up syntheses

Reactants	Solvent	T, t	Shape	Ref
$FeCl_2$(100 °C) + S	OLA[a]	180 °C, 1 h	Nanoparticle	86
$FeCl_2$ + S	HDA[b] + OLA[a]	250 °C, 3 h + 200 °C, 9 h	Cube	7
Fe_2O_3 + S	OLA[a] + OA[c] + CTAB[d]	290 °C, 1 h	Cube	87
$FeCl_2$ + $Na_2S_2O_3$	DMSO[e] + TGA[f] + EDA[g]	139 °C, 2–12 h	Nanoparticle; nanowire; nanosheet	88
$FeSO_4$ + S	TEG[h]	200 °C, 4 h	Mesoporous microsphere	89
		200 °C, 20 h	Solid microsphere	89

[a] As oleylamine. [b] As hexadecylamine. [c] As oleic acid. [d] As hexadecyltrimethylammonium bromide. [e] As dimethyl sulfoxide. [f] As thioglycolic acid. [g] As ethylenediamine. [h] As triethyleneglycol.

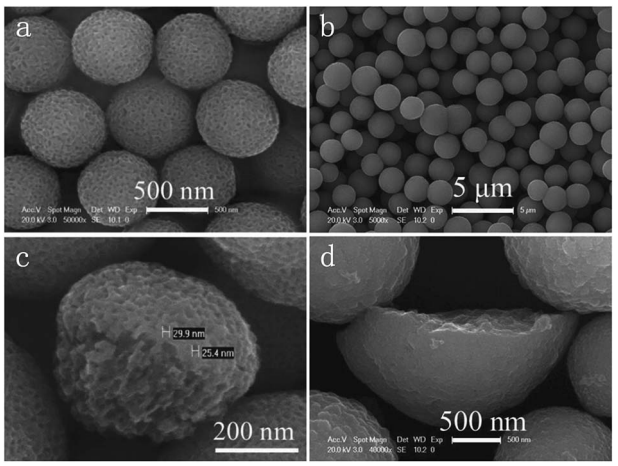

Fig. 6 SEM images of the honeycomb-like (a and c) and solid (b and d) FeS_2 microspheres.[89] Reprinted with permission from ref. 89. Copyright 2014 John Wiley & Sons, Inc.

can be observed that a variety of chemicals are employed as the precursor materials. Although the number of studies on the heat-up synthesis of iron pyrite are fewer than that of hot-injection synthesis, the selection range of the iron precursor, from $FeCl_2$ (ref. 7, 86 and 88) to Fe_2O_3 (ref. 87) and $FeSO_4$,[89] in the heat-up method is wider than that in the hot-injection method. Iron pyrite with various shapes, such as nanocubes, nanowires or nanosheets, can be obtained from the heat-up synthesis. Macpherson *et al.*[7] obtained iron pyrite nanocubes by employing the heat-up synthesis method with a second growth method. Bai *et al.*[88] managed to control the shape of iron pyrite form nanoparticles to nanowires and nanosheets by changing the molar ratio of the precursor Fe^{2+} and stabilizer, thioglycolic acid (TGA), from 1 : 4 to 1 : 3 or 1 : 2. Furthermore, Xu *et al.*[89] synthesized mesoporous (Fig. 6a and c) and solid microspherical (Fig. 6b and d) iron pyrite, by adjusting the reaction time from 4 h to 20 h.

3. Sulphidation synthesis of iron pyrite with different morphologies

Sulphidation synthesis is widely used to convert precursor materials, such as metal and oxides, to sulphides, which is significant to the formation of sulphide minerals.[90] It is also called as thermal sulphuration, sulphurization or sulphurating in some studies; sulphidation is the term that will be used during this review study. In a typical process, the precursor materials are initially prepared and, following that, thermal sulphidation is usually carried out at a certain temperature (between 200 and 600 °C), for a certain period of time (between several minutes to hours), under a sulphur or hydrogen sulphide (H_2S) atmosphere, using a tube reactor equipped with gas flow and pressure control options.

The synthesis of iron pyrite by thermal sulphidation has been popular since the 1980s, which was used for preparing iron pyrite for the manufacturing of solar devices. Many types of precursor materials have been employed in the reported studies, including iron films,[91–99] iron oxide films,[100–105] iron sulphide films[106,107] and other typical chemicals.[1,108–117] The terminal morphology of iron pyrite is determined by the precursor materials. When the precursor materials are films, nanotubes or nanowires, so are the terminal pyrite samples. Therefore, the previous studies could be classified into two classes, according to the morphology of pyrite. One would focus on iron pyrite films, while the other on nano iron pyrite with different morphology. However, only the latter is discussed below since the purpose of this review.

Table 5 summarizes the different morphologies, of nano iron pyrite, as reported in previous studies, synthesised by thermal sulphidation. It can be observed that the morphology of iron pyrite depends on the precursor. Some precursors were sulphured directly without any treatment. Amorim *et al.*[116] and Caban-Acevedo *et al.*[117,118] used Fe_2O_3, low-carbon steel and $FeCl_2 \cdot 4H_2O/FeBr_2$ powder as precursors, which were sulphured directly, to prepare iron pyrite spheres, nanowires, nanobelts and nanoplates. Some precursors were also prepared by various methods, including template,[119–121] solution synthesis[122] and anodization.[123]

When the precursors are prepared by a specific method, the products usually have the same or similar morphology with their precursors. For instance, Li *et al.*[122] used $FeF_3 \cdot 3H_2O$ nanowire, as precursor to prepare iron pyrite, prepared by solution synthesis, and the morphology of the products after sulphidation was also nanowires (Fig. 7a and b). In Wang *et al.*'s report,[121] ZnO nanorod arrays were used as the initial template

Table 5 Nano iron pyrite with different morphology from that of the reported thermal sulphidation synthesis

Precursor	Method	Sulphidation conditions	Morphology	Ref
Iron films	No	Ar plasma-assisted in S	nr[d]	124
Fe nw[b]	EP[a] + AAO template	300 to 450 °C for 8 h in S	nw[b] arrays	119
Fe_2O_3	No	400–500 °C in S	Quasi sphere	116
Low-carbon steel	No	350 °C for 20 h in S/H_2S	nw[b]	118
$FeCl_2 \cdot 4H_2O$/$FeBr_2$ powder	No	425 °C for 45 min in S	nr[d], nb[e], np[f]	117
$FeF_3 \cdot 3H_2O$ nw[b]	Solution synthesis	500 °C for 2 h in S	nw[b]	122
Fe_2O_3 nw[b]	AAO template	500 °C for 1 h in S	nw[b], nt[c]	120
$Fe(OH)_3$ nt[c]	ZnO template	350 °C for 3 h in S	nr[d] arrays	121
Fe_3O_4 nt[c]	Anodization	400 °C for 5 h in S	nt[c]	123

[a] As electrodeposition. [b] As nanowire. [c] As nanotube. [d] As nanorod. [e] As nanobelt. [f] As nanoplate.

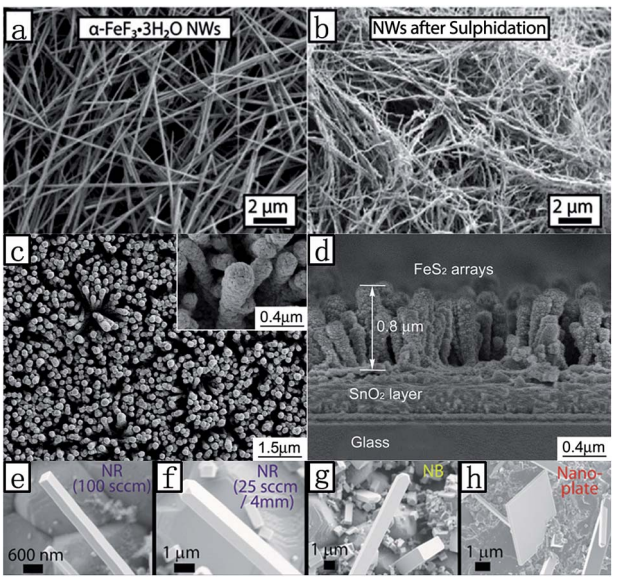

Fig. 7 SEM images of the NWs before (a) and after sulphidation (b),[122] and FeS_2 nanorod arrays: (c) top view and (d) cross-sectional view;[121] (e and f) NR, (g) NB and (h) nanoplate.[117] Reprinted with permission from ref. 117. Copyright 2013 American Chemical Society and ref. 121 and 122. Copyright 2014 Royal Society of Chemistry.

to produce $Fe(OH)_3$ nanotube arrays and then the $Fe(OH)_3$ nanotube arrays were used as a template to produce the final iron pyrite nanorod arrays (Fig. 7c and d).

When the precursors are sulphured without any further treatment, the morphology of products is usually different to that of their precursors. Cabán-Acevedo *et al.*[117,118] used low-carbon steel and $FeCl_2 \cdot 4H_2O$ or $FeBr_2$ powder as precursors to prepare iron pyrite. The morphology of the products was amazingly different to that of the precursors: nanowire, nanorod, nanobelt and nanoplate were able to be obtained (Fig. 7e–h).

The existing literature about this method can be considered as the beginning to the new-fangled iron pyrite nanomaterials world. The morphology of iron pyrite, prepared from sulphidation synthesis, can be controlled by adjusting different precursors or different preparation methods. This method could be an important method for the preparation of novel iron pyrite nanomaterials.

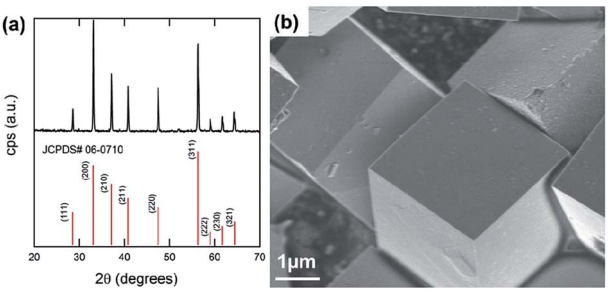

Fig. 8 (a) Indexed X-ray diffraction of synthetic cubic-FeS_2. (b) FESEM image of synthetic cubic-FeS_2 that confirms cubic structure with 2–3 μm cubes.[132] Reprinted with permission from ref. 132. Copyright 2012 John Wiley & Sons, Inc.

4. Synthesis of iron pyrite with other methods of relatively high efficiency

Except for the above methods to synthesize iron pyrite with the desired morphologies, the synthesis of iron pyrite with other, of relatively higher efficiency methods, were also carried out. The sputtering deposition,[125–129] microwave,[130–132] plasma,[91,124] magnetic field,[133] electrochemical deposition,[134] pulsed electron ablation[135] and mechanical milling[136] were employed to synthesize iron pyrite. However, not all of these highly efficient methods could be the appropriate ones to synthesize iron pyrite crystals with the designed morphologies.

A special morphology could be obtained when the microwave or magnetic field methods are employed. Kim and Batchelor,[130] successfully synthesized iron pyrite within a few minutes, through the reaction of ferric iron and hydrogen sulphide, under the influence of irradiation by a conventional microwave oven. Aided by microwaves, monodisperse iron pyrite microspheres[131] and cubic iron pyrite crystals (Fig. 8)[132] could be obtained. Aided by magnetic field, Wei *et al.* obtained iron pyrite sponge-like nanochained networks.

5. Summary and outlook

As a conclusion, monodisperse iron pyrite crystals, spheres and nano arrays could be obtained by employing the summarized methods above. Merits could be found in these synthetic routes.

To fabricate micro- or nano-iron pyrite mono-crystals with monomorphous facets, the wet-chemical routes, *i.e.* the hydrothermal, solvothermal, hot-injection and heat-up methods, are appropriate for controlling the size and shape. Most particularly, the hot-injection method is efficient for monodisperse narrow size distribution. If attempting to do so with any other methods of higher efficiency, it may be more helpful to tune the facets. Compared to the wet-chemical routes, the sulphidation method would be easier to operate and synthesize polycrystalline iron pyrite with diverse morphologies. However, it is hard to synthesize iron pyrite mono crystals from sulphidation. Due to the lowest surface energy, the cubic iron pyrite planes of {100} are much easier synthesized and more regular than other synthetic facets, like the octahedral {111}. To obtain iron pyrite polycrystals with different morphologies, such as iron pyrite nanoarrays or nanowires, a designed precursor template should be employed for the sulphidation method.

Compared to other semiconductor photocatalysts, such as TiO_2,[46] the relative research studies on crystal facet engineering of iron pyrite is at early stages. Nowadays, the crystal facet engineering of semiconductors has become an important strategy for defining the physicochemical properties and thus optimizing the reactivity and selectivity of photocatalysts,[49] the crystal facet engineering of iron pyrite could become a valid strategy for fine-tuning of the photovoltaic and environmental properties. Therefore, the new target area of iron pyrite syntheses should be focused on the iron pyrite crystals with tailored facets.

Although some facets, such as the cubic {100} and the octahedral {111}, of iron pyrite have been synthesized in previous studies, some challenges are still not overcome, for well tuning the crystal facets of iron pyrite. Some challenges and probable solutions are listed below: (i) the interactive mode and force between the surfactants or solvents with iron pyrite crystalline facets are not clear. Computational simulations should be performed to provide guidelines to the choice of suitable surfactants or solvents. (ii) The suitability of inorganic ions for capping agents, like F^- for anatase {100} facets,[137] to achieve various shapes should be examined. Only when a significant volume of experiments has been carried out, should this issue be resolved roundly. (iii) The driving force and acting form of the OA mechanism in iron pyrite crystal growth processes are also other issues that remain to be clarified. (iv) The relationship between the precursor materials and pH with the evolution of iron pyrite shape is another issue which should be disclosed, based on well-designed experiments. This may be a potential approach to transform the synthetic iron pyrite from octahedral {111} to a more regular.

Acknowledgements

This work was supported by the National Natural Science Foundation of China (Grant No. 41573112) and Youth Innovation Promotion Association CAS (Grant No. 2014324). This is a contribution No. IS-2210 from GIGCAS. We thank the anonymous referees for their heroic efforts and constructive comments on an earlier version of this paper, which did much to improve the manuscript.

References

1 S. Nakamura and A. Yamamoto, *Sol. Energy Mater. Sol. Cells*, 2001, **65**, 79–85.
2 Y. Bi, Y. Yuan, C. L. Exstrom, S. A. Darveau and J. Huang, *Nano Lett.*, 2011, **11**, 4953–4957.
3 M. A. Khan, J. C. Sarker, S. Lee, S. C. Mangham and M. O. Manasreh, *Mater. Chem. Phys.*, 2014, **148**, 1022–1028.
4 S. C. Mangham, M. A. Khan, M. Benamara and M. O. Manasreh, *Mater. Lett.*, 2013, **97**, 144–147.
5 J. Puthussery, S. Seefeld, N. Berry, M. Gibbs and M. Law, *J. Am. Chem. Soc.*, 2011, **133**, 716–719.
6 P. Namanu, M. Jayalakshmi and K. U. Bhat, *J. Mater. Sci.: Mater. Electron.*, 2015, **26**, 8534–8539.
7 H. A. Macpherson and C. R. Stoldt, *ACS Nano*, 2012, **6**, 8940–8949.
8 P. Kush, N. C. Mehra and S. Deka, *Sci. Adv. Mater.*, 2013, **5**, 788–795.
9 R. Murphy and D. R. Strongin, *Surf. Sci. Rep.*, 2009, **64**, 1–45.
10 T. H. Chen, J. Z. Wang, J. Wang, J. J. Xie, C. Z. Zhu and X. M. Zhan, *Int. J. Environ. Sci. Technol.*, 2015, **12**, 885–892.
11 C. Kantar, C. Ari and S. Keskin, *Water Res.*, 2015, **76**, 66–75.
12 C. Kantar, C. Ari, S. Keskin, Z. G. Dogaroglu, A. Karadeniz and A. Alten, *J. Contam. Hydrol.*, 2015, **174**, 28–38.
13 L. H. Kong, X. Y. Hu and M. C. He, *Environ. Sci. Technol.*, 2015, **49**, 3499–3505.
14 H. F. Liu, T. W. Qian and M. G. Zhang, *Spectrosc. Spectral Anal.*, 2015, **35**, 543–546.
15 P. Pourghahramani and B. N. Akhgar, *J. Ind. Eng. Chem.*, 2015, **25**, 131–137.
16 S. Ammar, M. A. Oturan, L. Labiadh, A. Guersalli, R. Abdelhedi, N. Oturan and E. Brillas, *Water Res.*, 2015, **74**, 77–87.
17 L. Labiadh, M. A. Oturan, M. Panizza, N. B. Hamadi and S. Ammar, *J. Hazard. Mater.*, 2015, **297**, 34–41.
18 L. Reyes-Bozo, M. Escudey, E. Vyhmeister, P. Higueras, A. Godoy-Faundez, J. L. Salazar, H. Valdes-Gonzalez, G. Wolf-Sepulveda and R. Herrera-Urbina, *Miner. Eng.*, 2015, **78**, 128–135.
19 M. Sanchez-Arenillas and E. Mateo-Marti, *Chem. Phys.*, 2015, **458**, 92–98.
20 Y. Q. Zhang, H. P. Tran, I. Hussain, Y. Q. Zhong and S. B. Huang, *Chem. Eng. J.*, 2015, **279**, 396–401.
21 W. L. Bragg, *Proc. R. Soc. London, Ser. A*, 1914, **89**, 468–489.
22 G. Chen, D. Sun, L. Zhang, W. Zang, J. Wang and A. Lu, *Geoscience*, 1987, **1**, 60–76.
23 J. A. Wilson, *Adv. Phys.*, 1972, **21**, 143–198.
24 E. T. Allen, J. L. Crenshaw, J. Johnston and E. S. Larsen, *Am. J. Sci.*, 1912, **33**, 169–236.
25 H. Ohfuji and D. Rickard, *Earth-Sci. Rev.*, 2005, **71**, 147–170.
26 K. Byrappa and M. Yoshimura, *Handbook of hydrothermal technology*, William Andrew, 2012.
27 H. Duan, Y. F. Zheng, Y. Z. Dong, X. G. Zhang and Y. F. Sun, *Mater. Res. Bull.*, 2004, **39**, 1861–1868.

28 R. Wu, Y. F. Zheng, X. G. Zhang, Y. F. Sun, J. B. Xu and J. K. Jian, *J. Cryst. Growth*, 2004, **266**, 523–527.
29 X. Feng, X. M. He, W. H. Pu, C. Y. Jiang and C. R. Wan, *Ionics*, 2007, **13**, 375–377.
30 D. Zhang, X. Wang, Y. Mai, X. Xia, C. Gu and J. Tu, *J. Appl. Electrochem.*, 2012, **42**, 263–269.
31 J. Zou and J. C. Gao, *Mater. Sci. Forum*, 2009, **610–613**, 459–462.
32 X. Q. Qiu, M. Liu, T. Hayashi, M. Miyauchi and K. Hashimoto, *Chem. Commun.*, 2013, **49**, 1232–1234.
33 D. Wang, Q. Wang and T. Wang, *CrystEngComm*, 2010, **12**, 3797–3805.
34 L. Zhu, B. Richardson, J. Tanumihardja and Q. Yu, *CrystEngComm*, 2012, **14**, 4188–4195.
35 X. Chen, Z. Wang, X. Wang, J. Wan, J. Liu and Y. Qian, *Inorg. Chem.*, 2005, **44**, 951–954.
36 Y. Hu, Z. Zheng, H. M. Jia, Y. W. Tang and L. Z. Zhang, *J. Phys. Chem. C*, 2008, **112**, 13037–13042.
37 C. Wadia, Y. Wu, S. Gul, S. K. Volkman, J. H. Guo and A. P. Alivisatos, *Chem. Mater.*, 2009, **21**, 2568–2570.
38 J. Xia, J. Q. Jiao, B. L. Dai, W. D. Qiu, S. X. He, W. T. Qiu, P. K. Shen and L. P. Chen, *RSC Adv*, 2013, **3**, 6132–6140.
39 Z. T. Yang, X. J. Liu, J. S. Liu and X. L. Feng, *Key Eng. Mater.*, 2013, **562–565**, 136–140.
40 Z. T. Yang, X. J. Liu, X. L. Feng, Y. X. Cui and X. W. Yang, *J. Appl. Electrochem.*, 2014, **44**, 1075–1080.
41 A. Akhoondi, M. Ziarati and N. Khandan, *Iran. J. Chem. Chem. Eng.*, 2014, **33**, 15–19.
42 S. Middya, A. Layek, A. Dey and P. P. Ray, *J. Mater. Sci. Technol.*, 2014, **30**, 770–775.
43 B. X. Yuan, W. L. Luan and S. T. Tu, *Mater. Lett.*, 2015, **142**, 160–162.
44 B. X. Yuan, W. L. Luan, S. T. Tu and J. Wu, *New J. Chem.*, 2015, **39**, 3571–3577.
45 S. T. Liu, J. Wu, P. Yu, Q. H. Ding, Z. H. Zhou, H. D. Li, C. C. Lai, Y. L. Chueh and Z. M. M. Wang, *Nanoscale Res. Lett.*, 2014, **9**, 549–555.
46 G. Liu, H. G. Yang, J. Pan, Y. Q. Yang, G. Q. Lu and H. M. Cheng, *Chem. Rev.*, 2014, **114**, 9559–9612.
47 A. Hung, J. Muscat, I. Yarovsky and S. P. Russo, *Surf. Sci.*, 2002, **513**, 511–524.
48 A. Hung, J. Muscat, I. Yarovsky and S. P. Russo, *Surf. Sci.*, 2002, **520**, 111–119.
49 G. Liu, J. C. Yu, G. Q. Lu and H. M. Cheng, *Chem. Commun.*, 2011, **47**, 6763–6783.
50 N. E'jazi and M. Aghaziarati, *Adv. Powder Technol.*, 2012, **23**, 352–357.
51 X. Qian, Y. Xie and Y. Qian, *Mater. Lett.*, 2001, **48**, 109–111.
52 S. Kar and S. Chaudhuri, *Chem. Phys. Lett.*, 2004, **398**, 22–26.
53 S. Kar and S. Chaudhuri, *Mater. Lett.*, 2005, **59**, 289–292.
54 B.-B. Yu, X. Zhang, Y. Jiang, J. Liu, L. Gu, J.-S. Hu and L.-J. Wan, *J. Am. Chem. Soc.*, 2015, **137**, 2211–2214.
55 H. Ma, Z. G. Zou, Y. Wu, F. Long, H. J. Yu and C. Y. Xie, *Adv. Mater. Res.*, 2011, **287–290**, 1327–1330.
56 D. Wang, M. Wu, Q. Wang, T. Wang and J. Chen, *Ionics*, 2011, **17**, 163–167.
57 Y. H. Chen, Y. F. Zheng, X. G. Zhang, Y. F. Sun and Y. Z. Dong, *Sci. China, Ser. G: Phys., Mech. Astron.*, 2005, **48**, 188–200.
58 D. Wang, Q. Wang and T. Wang, *CrystEngComm*, 2010, **12**, 755–761.
59 R. Wu, J. K. Jian, L. T. Tao, Y. L. Bian, J. Li, Y. F. Sun, J. Wang and X. Y. Zeng, *Powder Diffr.*, 2010, **25**, S40–S44.
60 S. L. Liu, M. M. Li, S. Li, H. L. Li and L. Yan, *Appl. Surf. Sci.*, 2013, **268**, 213–217.
61 W. L. Liu, X. H. Rui, H. T. Tan, C. Xu, Q. Y. Yan and H. H. Hng, *RSC Adv.*, 2014, **4**, 48770–48776.
62 T. S. Yoder, J. E. Cloud, G. J. Leong, D. F. Molk, M. Tussing, J. Miorelli, C. Ngo, S. Kodambaka, M. E. Eberhart, R. M. Richards and Y. A. Yang, *Chem. Mater.*, 2014, **26**, 6743–6751.
63 Y. Chen, Y. Zheng, X. Zhang, Y. Sun and Y. Dong, *Sci. China: Phys., Mech. Astron.*, 2005, **48**, 188–200.
64 C. B. Murray, D. J. Norris and M. G. Bawendi, *J. Am. Chem. Soc.*, 1993, **115**, 8706–8715.
65 S. G. Kwon and T. Hyeon, *Small*, 2011, **7**, 2685–2702.
66 J. Joo, H. B. Na, T. Yu, J. H. Yu, Y. W. Kim, F. X. Wu, J. Z. Zhang and T. Hyeon, *J. Am. Chem. Soc.*, 2003, **125**, 11100–11105.
67 W. Li, M. Doblinger, A. Vaneski, A. L. Rogach, F. Jackel and J. Feldmann, *J. Mater. Chem.*, 2011, **21**, 17946–17952.
68 J. Park, J. Joo, S. G. Kwon, Y. Jang and T. Hyeon, *Angew. Chem., Int. Ed.*, 2007, **46**, 4630–4660.
69 L. K. Ganta, T. P. Dhakal, S. Rajendran and C. R. Westgate, *in Synthesis of FeS_2 Nano Crystals for Ink-Based Solar Cells, MRS Proceedings*, Cambridge Univ Press, 2012, pp mrss12-1447-v07-06.
70 A. Kirkeminde, B. A. Ruzicka, R. Wang, S. Puna, H. Zhao and S. Ren, *ACS Appl. Mater. Interfaces*, 2012, **4**, 1174–1177.
71 K. P. Bhandari, P. J. Roland, T. Kinner, Y. Cao, H. Choi, S. Jeong and R. J. Ellingson, *J. Mater. Chem. A*, 2015, **3**, 6853–6861.
72 J. M. Lucas, C. C. Tuan, S. D. Lounis, D. K. Britt, R. M. Qiao, W. Yang, A. Lanzara and A. P. Alivisatos, *Chem. Mater.*, 2013, **25**, 1615–1620.
73 M. Gong, A. Kirkeminde and S. Ren, *Sci. Rep.*, 2013, **3**, 1–6.
74 D. Y. Wang, Y. T. Jiang, C. C. Lin, S. S. Li, Y. T. Wang, C. C. Chen and C. W. Chen, *Adv. Mater.*, 2012, **24**, 3415–3420.
75 B. Kilic, J. Roehling and O. T. Ozmen, *J. Nanoelectron. Optoelectron.*, 2013, **8**, 260–266.
76 A. Kirkeminde and S. Q. Ren, *J. Mater. Chem. A*, 2013, **1**, 49–54.
77 H. Ge, L. Hai, R. R. Prabhakar, L. Y. Ming and T. Sritharan, *RSC Adv.*, 2014, **4**, 16489–16496.
78 M. A. Khan and Y. M. Kang, *Mater. Lett.*, 2014, **132**, 273–276.
79 M. A. Khan, M. O. Manasreh and Y. M. Kang, *Mater. Lett.*, 2014, **126**, 181–184.
80 H. T. Kim, T. P. N. Nguyen, C. Kim and C. Park, *Mater. Chem. Phys.*, 2014, **148**, 1095–1098.
81 W. Li, T. Dittrich, F. Jäckel and J. Feldmann, *Small*, 2014, **10**, 1194–1201.

82 L. Z. Zhu, B. J. Richardson and Q. M. Yu, *Nanoscale*, 2014, **6**, 1029–1037.
83 F. Jiang, L. T. Peckler and A. J. Muscat, *Cryst. Growth Des.*, 2015, **15**, 3565–3572.
84 N. T. N. Truong, T. P. N. Nguyen, V. T. H. Pham, K. T. Trinh, S. H. Lee and C. Park, *Jpn. J. Appl. Phys.*, 2015, **54**, 045001.
85 L. Zhu, B. J. Richardson and Q. Yu, *Chem. Mater.*, 2015, **27**(9), 3516–3525.
86 S. C. Hsiao, C. M. Hsu, S. Y. Chen, Y. H. Perng, Y. L. Chueh, L. J. Chen and L. H. Chou, *Mater. Lett.*, 2012, **75**, 152–154.
87 B. X. Yuan, W. L. Luan and S. T. Tu, *Dalton Trans.*, 2012, **41**, 772–776.
88 Y. X. Bai, J. Yeom, M. Yang, S. H. Cha, K. Sun and N. A. Kotov, *J. Phys. Chem. C*, 2013, **117**, 2567–2573.
89 J. Xu, H. T. Xue, X. Yang, H. X. Wei, W. Y. Li, Z. P. Li, W. J. Zhang and C. S. Lee, *Small*, 2014, **10**, 4754–4759.
90 R. H. Sillitoe, *Econ. Geol.*, 2010, **105**, 3–41.
91 S. Bausch, B. Sailer, H. Keppner, G. Willeke, E. Bucher and G. Frommeyer, *Appl. Phys. Lett.*, 1990, **57**, 25–27.
92 B. Rezig, H. Dahman and M. Kenzari, *Renewable Energy*, 1992, **2**, 125–128.
93 L. Meng, Y. H. Liu and W. Huang, *Mater. Sci. Eng., B*, 2002, **90**, 84–89.
94 L. Meng, Y. H. Liu and L. Tian, *J. Cryst. Growth*, 2003, **253**, 530–538.
95 L. Meng, Y. H. Liu and L. Tian, *Mater. Res. Bull.*, 2003, **38**, 941–948.
96 L. Y. Huang, Y. H. Liu and L. Meng, *J. Mater. Sci. Technol.*, 2009, **25**, 237–241.
97 L. Y. Huang and L. Meng, *Mater. Chem. Phys.*, 2010, **124**, 413–416.
98 Z. J. Luan, Y. Wang, L. Y. Huang, F. Wang and L. Meng, *Mater. Res. Innovations*, 2011, **15**, 349–351.
99 J. M. LaForge, B. Gyenes, S. J. Xu, L. K. Haynes, L. V. Titova, F. A. Hegmann and M. J. Brett, *Sol. Energy Mater. Sol. Cells*, 2013, **117**, 306–314.
100 G. Smestad, A. Ennaoui, S. Fiechter, H. Tributsch, W. K. Hofmann, M. Birkholz and W. Kautek, *Sol. Energy Mater.*, 1990, **20**, 149–165.
101 L. Y. Huang, F. Wang, Z. J. Luan and L. A. Meng, *Mater. Lett.*, 2010, **64**, 2612–2615.
102 Z. J. Luan, L. Y. Huang, F. Wang and L. Meng, *Appl. Surf. Sci.*, 2011, **258**, 1505–1509.
103 Z. J. Luan, F. Wang, D. W. Yao, L. Y. Huang and L. Meng, *Mater. Res. Bull.*, 2011, **46**, 1577–1581.
104 F. Wang, L. Y. Huang, Z. J. Luan, J. S. Huang and L. Meng, *Mater. Chem. Phys.*, 2012, **132**, 505–508.
105 K. W. Sun, Z. H. Su, J. Yang, Z. L. Han, F. Y. Liu, Y. Lai, J. Li and Y. X. Liu, *Thin Solid Films*, 2013, **542**, 123–128.
106 H. F. Liu and D. Z. Chi, *J. Vac. Sci. Technol., A*, 2012, **30**, 04D102.
107 A. Kirkeminde, P. Gingrich, M. G. Gong, H. Z. Cui and S. Q. Ren, *Nanotechnology*, 2014, **25**, 205603.
108 A. K. Abass, Z. A. Ahmed and R. E. Tahir, *Phys. Status Solidi A*, 1986, **97**, 243–247.
109 G. Chatzitheodorou, S. Fiechter, M. Kunst, J. Luck and H. Tributsch, *Mater. Res. Bull.*, 1988, **23**, 1261–1271.
110 G. Smestad, A. Da Silva, H. Tributsch, S. Fiechter, M. Kunst, N. Meziani and M. Birkholz, *Sol. Energy Mater.*, 1989, **18**, 299–313.
111 A. Gomes, J. R. Ares, I. J. Ferrer, M. I. D. Pereira and C. Sanchez, *Mater. Res. Bull.*, 2003, **38**, 1123–1133.
112 A. Yamamoto, M. Nakamura, A. Seki, E. L. Li, A. Hashimoto and S. Nakamura, *Sol. Energy Mater. Sol. Cells*, 2003, **75**, 451–456.
113 Y. Z. Dong, Y. Zheng, H. Duan, Y. Sun and Y. Chen, *Mater. Lett.*, 2005, **59**, 2398–2402.
114 Y. Z. Dong, Y. F. Zheng, X. G. Zhang, H. Duan, Y. F. Sun and Y. H. Chen, *Sci. China, Ser. E: Eng. Mater. Sci.*, 2005, **48**, 601–611.
115 B. Ouertani, J. Ouerfelli, M. Saadoun, B. Bessais, H. Ezzaouia and J. C. Bernede, *Mater. Charact.*, 2005, **54**, 431–437.
116 B. V. D. L. Amorim, F. J. Moura, E. A. Brocchi, M. J. P. Vieira and M. T. D. Rupp, *Metall. Mater. Trans. B*, 2012, **43**, 781–786.
117 M. Cabán-Acevedo, D. Liang, K. S. Chew, J. P. DeGrave, N. S. Kaiser and S. Jin, *ACS Nano*, 2013, **7**, 1731–1739.
118 M. Caban-Acevedo, M. S. Faber, Y. Z. Tan, R. J. Hamers and S. Jin, *Nano Lett.*, 2012, **12**, 1977–1982.
119 D. Y. Wan, Y. T. Wang, Z. P. Zhou, G. Q. Yang, B. Y. Wang and L. Wei, *Mater. Sci. Eng., B*, 2005, **122**, 156–159.
120 Y. Li, Z. L. Han, L. X. Jiang, Z. H. Su, F. Y. Liu, Y. Q. Lai and Y. X. Liu, *J. Sol-Gel Sci. Technol.*, 2014, **72**, 100–105.
121 M. D. Wang, C. C. Xing, K. Cao, L. Zhang, J. B. Liu and L. Meng, *J. Mater. Chem. A*, 2014, **2**, 9496–9505.
122 L. S. Li, M. Caban-Acevedo, S. N. Girard and S. Jin, *Nanoscale*, 2014, **6**, 2112–2118.
123 X. G. Shi, A. Tian, X. X. Xue, H. Yang and Q. Xu, *Mater. Lett.*, 2015, **141**, 104–106.
124 R. Morrish, R. Silverstein and C. A. Wolden, *J. Am. Chem. Soc.*, 2012, **134**, 17854–17857.
125 D. Lichtenberger, K. Ellmer, R. Schieck and S. Fiechter, *Appl. Surf. Sci.*, 1993, **70–1**, 583–587.
126 D. Lichtenberger, K. Ellmer, R. Schieck, S. Fiechter and H. Tributsch, *Thin Solid Films*, 1994, **246**, 6–12.
127 G. Willeke, R. Dasbach, B. Sailer and E. Bucher, *Thin Solid Films*, 1992, **213**, 271–276.
128 A. Baruth, M. Manno, D. Narasimhan, A. Shankar, X. Zhang, M. Johnson, E. S. Aydil and C. Leighton, *J. Appl. Phys.*, 2012, **112**, 054328.
129 M. Birkholz, D. Lichtenberger, C. Hopfner and S. Fiechter, *Sol. Energy Mater. Sol. Cells*, 1992, **27**, 243–251.
130 E. J. Kim and B. Batchelor, *Mater. Res. Bull.*, 2009, **44**, 1553–1558.
131 M. L. Li, Q. Z. Yao, G. T. Zhou, X. F. Qu, C. F. Mu and S. Q. Fu, *CrystEngComm*, 2011, **13**, 5936–5942.
132 T. A. Yersak, H. A. Macpherson, S. C. Kim, V. D. Le, C. S. Kang, S. B. Son, Y. H. Kim, J. E. Trevey, K. H. Oh, C. Stoldt and S. H. Lee, *Adv. Energy Mater.*, 2013, **3**, 120–127.
133 Z. H. Wei, Y. C. Qiu, H. N. Chen, K. Y. Yan, Z. L. Zhu, Q. Kuang and S. H. Yang, *J. Mater. Chem. A*, 2014, **2**, 5508–5515.

134 B. Chakraborty, B. Show, S. Jana, B. C. Mitra, S. K. Maji, B. Adhikary, N. Mukherjee and A. Mondal, *Electrochim. Acta*, 2013, **94**, 7–15.
135 R. Henda, O. Al-Shareeda, A. McDonald and A. Pratt, *Appl. Phys. A: Mater. Sci. Process.*, 2012, **108**, 967–974.
136 P. P. Chin, J. Ding, J. B. Yi and B. H. Liu, *J. Alloys Compd.*, 2005, **390**, 255–260.
137 H. G. Yang, C. H. Sun, S. Z. Qiao, J. Zou, G. Liu, S. C. Smith, H. M. Cheng and G. Q. Lu, *Nature*, 2008, **453**, 638–641.